

# Analytical Dynamical Models for Double-Power-Law Galactic Nuclei

HongSheng Zhao

Max-Planck-Institute für Astrophysik, 85740 Garching, Germany

Email: hsz@MPA-Garching.MPG.DE

## ABSTRACT

Motivated by the finding that the observed surface brightness profile of many galactic nuclei are well fit by double-power-laws, we explore a range of spherical self-consistent dynamical models with this light profile.

We find that the corresponding deprojected volume density profile, phase space density and line-of-sight velocity distribution of these models are well fit by simple analytic approximations. We illustrate the application of these models by fitting a sample of about 25 galactic nuclei observed by Hubble Space Telescope. We give the derived volume density, phase space density, velocity dispersion and line profile parameters in tables. The models are useful for predicting kinematic properties of these galaxies for comparison with future observations. They can also be easily applied to seed N-body simulations of galactic nuclei with realistic density profiles for studying the evolution of these systems.

*Subject headings:* galaxies: kinematics and dynamics - line: profiles

Submitted to Monthly Notices of R.A.S.

## 1. Introduction

Recent high-resolution observations of galactic nuclei find that their surface brightness profiles are well fit by a three-parameter double-power-law. Assuming a constant mass-to-light ratio, this means that the projected mass density  $\mu(R)$  satisfies (Lauer et al. 1995, Byun et al. 1996)<sup>1</sup>

$$\mu(R) = \mu_0 \left(\frac{R}{B}\right)^{-\gamma_1} \left(1 + \left(\frac{R}{B}\right)^{\frac{1}{\alpha_1}}\right)^{-(\beta_1 - \gamma_1)\alpha_1}, \quad (1)$$

where  $\gamma_1$ ,  $\beta_1$  and  $\alpha_1$  specify the slope of the inner power-law, the outer power-law and the width of transition region. Meaningful values for the three parameters satisfy  $0 \leq \gamma_1 \leq \beta_1$  and  $\alpha_1 > 0$ . Other parameters  $B$ ,  $\mu_0$  are scaling parameters, specifying a length scale (the break radius) and a scale for projected density. For flattened nuclei, the parametrization applies on the major or minor axis or in a shell averaged sense.

Interpreting this class of density profiles requires a new class of dynamical models. Previous dynamical models mostly have a finite core. A recent set of cuspy models, including the  $\gamma/\eta$  models discovered by Dehnen (1994) and Tremaine et al. (1995), and a even wider range of analytical models by Zhao (1996), often do not match the light of nuclei outside the break radius. Unlike these models the observed light profiles are often much shallower at large radius, and in principle correspond to a divergent mass if extrapolated to infinity. Hence it is necessary to explore dynamical models consistent with a general double-power-law profile, including those with a divergent mass.

The existence of a universal parametrization constitutes a major advantage for theoretical study of their dynamical properties. It makes it possible to study observed galactic nuclei as a class spanned by the three slope parameters  $(\alpha_1, \beta_1, \gamma_1)$ , and constrain the models with the steady state dynamics without necessarily using data of individual systems explicitly. In this paper, we give some results which immediately follow from the above surface brightness profiles. We will concentrate on the simple class of spherical isotropic models with main emphasis on their simple analytical results.

While spherical models with a  $f(E)$  distribution function are famous for admitting mathematical solutions, and are often used as a compromise for more realistic but less tractable anisotropic/flattened/triaxial models, the actual implementation of the spherical models is in fact very tedious, and rarely admits simple analytical results. These

---

<sup>1</sup> The parameters  $\alpha_1, \beta_1, \gamma_1$  in this paper correspond to  $\frac{1}{\alpha}, \beta, \gamma$  respectively in the convention used by these authors. Their models are restricted to surface brightness studies to establish the central cusp in light.

significantly complicate the first-level simple interpretation of photometric and kinematic data. The standard inversion using Eddington formula involves at least three integrations and two derivatives (analytical or numerical) to get  $f(E)$  from a surface density profile. To further make a prediction on line profile requires computing a three dimensional integral (see e.g., Dehnen 1994) at each grid point in the projected radius vs. velocity plane.

For the current problem, one is interested in a class of models with a range of density profiles. The main challenge is to present the results in a manageable and easily interpretable way. Virtually no rigorous analytical solutions are known for the projected models given by Eq.(1). Even for some related analytical models (Zhao 1996, Dehnen 1994, Tremaine et al. 1995), the expressions of the distribution function and projected density and dispersion are generally very lengthy, typically involving more than half a dozen analytic terms with no clear physical meaning and with possible large cancellations between terms. As a result, the relations between observable and model quantities are obscured.

In this paper we build a set of spherical dynamical models with simple functional forms for the intrinsic volume density and  $f(E)$ . We fit these to the double-power-law projected density models. We set the scaling quantities,  $\mu_0$  and  $B$  as unity, and vary the dimensionless parameters  $(\alpha_1, \beta_1, \gamma_1)$  in a 3D parameter space to simulate a complete set of radial profiles of the surface light. Because of the way the fitted models are tailored, the residuals of the fits are typically smaller than the uncertainties in the data so that the models are practically consistent with the double-power-law surface brightness profile.

The main results of the paper are summarized in several universal formulae for the volume density, the phase space density, the line-of-sight velocity profiles. The model results can be presented directly with the fitting formulae and a few numerically fitted parameters.

To demonstrate the applications, we compute the system parameters for about 25 observed galaxies and give them in tables. With these the intrinsic and projected quantities of the model are fully determined, and it involves virtually no further calculation to predict the line-of-sight velocity distributions.

The paper is organized as follows. In Section 2 we fit the surface brightness profiles with analytical volume density models. Section 3 gives the analytical expression for the model potential. Section 4 gives the deprojected phase space density by matching the volume density and the potential. In Section 5, the distribution functions are re-projected to yield line-of-sight velocity distributions as well as the dispersion and kurtosis of the profiles, all on a grid of projected radius. We illustrate the model applications in Section 6. We summarize in Section 7. Asymptotic relations for the model quantities are given in Appendix A. Some alternative analytical approximations with rigorous asymptotic solutions

are given in Appendix B. A simple formula for the line profiles of the models is derived in Appendix C.

Although similar models can be built for anisotropic spherical systems with a black hole, and the techniques are also generalizable to oblate  $f(E, J_z)$  systems, we leave these generalized models for a later study (Zhao and Syer 1996). The three-dimensional  $(\alpha_1, \beta_1, \gamma_1)$  parameter space of the spherical models is already very big, and at least two more dimensions would be necessary to cover spherical models with black hole and anisotropy. Also while the isotropic models are most likely stable, many simulations are needed to examine the stability of anisotropic or black hole models before applying them to observations.

## 2. Deprojected volume density profile

One expects an asymptotic power-law in surface brightness to correspond to a (steeper) power-law in volume density. So the double-power-law of the observed surface brightness of galactic nuclei suggests that their volume density could be fit by a similar double-power-law,

$$\nu(r) = \nu_0 \left(\frac{r}{b}\right)^{-\gamma} \left(1 + \left(\frac{r}{b}\right)^{\frac{1}{\alpha}}\right)^{-(\beta-\gamma)\alpha}, \quad (2)$$

where the new parameters  $(\alpha, \beta, \gamma)$  and  $\nu_0$  and  $b$  have the same meaning as the five parameters in Eq. 1 except that they describe the volume density profile instead of the surface brightness profile. In Appendix A we give the relations between  $(\alpha, \beta, \gamma, \nu_0, b)$  and  $(\alpha_1, \beta_1, \gamma_1, \mu_0, B)$  based on matching the two densities at asymptotic large or small radii. But except for a few special cases<sup>2</sup>, the deprojected density of  $\mu(R)$  in Eq. 1 is generally not as simple as  $\nu(r)$  in Eq. 2.

Our approach is to match the two densities in the least squared sense. We fix the outer slope

$$\beta = \beta_1 + 1, \quad (3)$$

to enforce a good match at large radius. Then we tune the other four parameters  $\alpha, \gamma, \nu_0, b$  to fit the surface brightness to a high accuracy by minimizing the following r.m.s residual,

$$\delta_\mu = \left(\frac{1}{N_R} \sum_{i=0}^{N_R} [\log I(R_i) - \log \mu(R_i)]^2\right)^{\frac{1}{2}} \quad (4)$$

---

<sup>2</sup>for finite core models with  $\alpha = \alpha_1 = \frac{1}{2}$  and for single-power-law models

where

$$I(R) = 2 \int_0^{+\infty} \nu(\sqrt{R^2 + z^2}) dz \quad (5)$$

is the projected density of  $\nu(r)$ , and the fitting positions  $R_i$  and the number of fitting points  $N$  are given in Table 1.

The initial values for the fitting parameters are taken from the following approximate relations

$$\gamma \approx \gamma_e = \gamma_1 + 1 \text{ if } \gamma_1 > 0 \quad (6)$$

$$= [1 - \frac{1}{\alpha_1}, 0]_{max} \text{ if } \gamma_1 = 0 \quad (7)$$

to fit near the cusp, where  $\gamma_e$  is the expected exact asymptotic power for the density, and

$$\alpha \approx \alpha_1, \quad b \sim B, \quad (8)$$

to fit near the break radius, and

$$\nu_0 b^{-\beta} \sim \frac{\Gamma(\frac{\beta}{2})}{2\sqrt{\pi}\Gamma(\frac{\beta-1}{2})} \mu_0 B^{-\beta-1}, \quad (9)$$

to match the density normalization far away.

The first panel in Fig. 1, Fig. 3 and Fig. 5 shows a few typical model fits and the upper panel of Fig. 6 shows their residuals. The residual is small over 4 or more decades in the intensity scale. The typical residual  $|\log I(R) - \log \mu(R)| \sim \delta_\mu$  is  $10^{-4} - 10^{-1}$  for the projected radius  $0.01 \leq R/B \leq 100$ . For galactic nuclei observed by Space Telescope the light is measured to an accuracy of about 0.1 magnitude ( $\sim 4\%$  difference in ten log) from the central  $0.1''$  to  $10''$  outward, with a typical break radius at  $1''$ . So the small internal residuals of the models here are negligible when fitting the photometric data. The above results are independent of the dynamics.

### 3. The potential

Zhao (1996) shows that the potential  $\phi(r) = -\Phi(r)$  corresponding to a double-power-law volume density distribution  $\nu(r)$  is simply a sum of two (analytical) incomplete Beta-functions (Zhao 1996).

$$\Phi(r) = 4\pi\nu_0 b^2 \alpha \left[ \frac{b}{r} B(\alpha(3-\gamma), \alpha(\beta-3), \frac{(\frac{r}{b})^{\frac{1}{\alpha}}}{1 + (\frac{r}{b})^{\frac{1}{\alpha}}}) + B(\alpha(\beta-2), \alpha(2-\gamma), \frac{1}{1 + (\frac{r}{b})^{\frac{1}{\alpha}}}) \right], \quad (10)$$

where the gravitational constant  $G$  is set to unity.

As the incomplete Beta-functions can be computed with a fast function call to standard routines in Numerical Recipes (Press et al. 1992), this greatly simplifies the numerics for the dynamics.

According to the asymptotic expression for  $\Phi(r)$  given in Appendix A, the zero point of the potential is at infinitely large radius. The depth of the potential well  $\Phi_0 = \Phi(0) > 0$  is infinite for models with a strong cusp with  $\gamma \geq 2$  (or if there is a central black hole), and is finite for  $\gamma < 2$ .

#### 4. Deprojected distribution function

In this section, we derive an approximation to the underlying intrinsic distribution function of the double-power law spherical density models. For simplicity we consider only models with isotropic velocity distribution, namely, models with distribution function  $f = f(Q)$ , where we define a positive energy  $0 \leq Q \leq \Phi(0)$  with

$$Q \equiv -E = \Phi(r) - \frac{1}{2}v^2, \quad (11)$$

and a function  $G(Q)$  being an integration of the  $f(Q)$ ,

$$G(Q) \equiv \int_0^Q f(Q)dQ. \quad (12)$$

To decide a functional form for  $f$  or  $G(Q)$ , we note that the distribution function of asymptotic power-law systems is often a power-law of energy at asymptotically large or small radius. For example, in the Hernquist model,  $f(Q) \propto Q^{5/2}$  at large radius and  $f(Q) \propto (\Phi_0 - Q)^{5/2}$  at small radius. So a sensible universal formula for the distribution function of the double-power-law density models should be a smooth positive function of  $Q$  which reduces to a power-law at small  $Q$  and large  $Q$ .

The following contrived expression for  $G(Q)$  has the desired property

$$G(Q) = f_0 Q_b q^{\beta_2} \left(1 + q^{\frac{1}{\alpha_2}}\right)^{(\gamma_2 - \beta_2)\alpha_2}, \quad (13)$$

where  $f_0$  and  $Q_b$  are two scaling quantities with the dimension of phase density and energy,  $(\alpha_2, \beta_2, \gamma_2)$  are another three dimensionless quantities for the shape of the distribution. We define a dimensionless energy  $q$ , which is a rescaling of the energy  $Q$  with

$$q \equiv \frac{\frac{Q}{Q_b}}{1 - \frac{Q}{\Phi_0}}, \text{ for finite potential well,} \quad (14)$$

$$\equiv \frac{Q}{Q_b}, \text{ for infinitely deep potential well,} \quad (15)$$

so that  $q$  runs from 0 to  $\infty$  with decreasing radius for models with finite as well as infinitely deep potential well. Note smaller (bigger) values for  $Q$  or  $q$  correspond to bigger (smaller) radius, and  $G(Q)$  reduces to power-law of  $q$  at big  $q$  and at small  $q$ .

Taking the derivative of Eq. 13 we obtain the corresponding distribution function  $f(Q)$  as

$$f = f(Q) = f_0 q^{\beta_2 - 1} (1 + q^{\frac{1}{\alpha_2}})^{(\gamma_2 - \beta_2)\alpha_2} \times W \times U, \quad (16)$$

where

$$W \equiv \gamma_2 + \frac{\beta_2 - \gamma_2}{1 + q^{\frac{1}{\alpha_2}}}, \quad (17)$$

and

$$U \equiv \frac{1}{(1 - \frac{Q}{\Phi_0})^2} = (1 + q \frac{Q_b}{\Phi_0})^2, \text{ for finite potential well,} \quad (18)$$

$$\equiv 1, \text{ for infinitely deep potential well,} \quad (19)$$

are two dimensionless factors.

It then follows from the above equation that  $f(Q)$  is positive definite given that  $\gamma_2 \geq 0$  and  $\beta_2 \geq 0$ , and has the following asymptotic power-law dependence on  $Q$ ,

$$f(Q) \propto Q^{\beta_2 - 1}, \quad Q \rightarrow 0 \quad (20)$$

$$\propto Q^{\gamma_2 - 1}, \quad Q \rightarrow \Phi_0 = \infty \quad (21)$$

$$\propto (\Phi_0 - Q)^{-\gamma_2 - 1}, \quad Q \rightarrow \text{a finite } \Phi_0 \text{ and } \gamma_2 > 0 \quad (22)$$

$$\propto 1, \quad Q \rightarrow \text{a finite } \Phi_0 \text{ and } \gamma_2 = 0. \quad (23)$$

To briefly comment on more general models, the parametrization for  $G(Q)$  or  $f(Q)$  is also plausible for models with a central black hole as  $f(Q)$  is a power-law for infinitely deep potential well (Tremaine et al. 1994). One can also obtain its simple counterpart in Osipkov-Merritt type anisotropic models if replacing  $Q$  with  $Q_a = -E - \frac{1}{2}\eta J^2$ .

For a given potential  $-\Phi(r)$ , the distribution function  $f(Q)$  has five fitting parameters  $(\alpha_2, \beta_2, \gamma_2, Q_b, f_0)$ . These are determined by making  $f(Q)$  and the volume density  $\nu(r)$  consistent. In practice we minimize the following r.m.s. residual,

$$\delta_\nu = \left( \frac{1}{N_r} \sum_{i=0}^{N_r} [\log n(r_i) - \log \nu(r_i)]^2 \right)^{\frac{1}{2}} \quad (24)$$

where the fitting positions  $r_i$  and the number of fitting points  $N_r$  are given in Table 1, and

$$n(r) = 4\pi\sqrt{2} \int_0^{\Phi(r)} f(Q)\sqrt{\Phi(r) - Q}dQ \quad (25)$$

is the volume density corresponding to  $f(Q)$  (cf. Binney and Tremaine 1987); after an integration of parts it reduces to a more convenient expression for  $n(r)$ :<sup>3</sup>

$$n(r) = 2\pi\sqrt{2} \int_0^{\Phi(r)} \frac{G(Q)}{\sqrt{\Phi(r) - Q}}dQ. \quad (26)$$

There are several simple (approximate) relations between the parameters  $(\alpha_2, \beta_2, \gamma_2, Q_b, f_0)$  and  $(\alpha, \beta, \gamma, b, \nu_0)$ , which follows from matching the densities  $\nu(r)$  and  $n(r)$  at big and small radius. If  $\beta_{2e}$  and  $\gamma_{2e}$  are the exact asymptotic powers for  $G(Q)$  as given in Appendix A, we require  $\beta_2 = \beta_{2e}$  in the fitting program. The true fitting parameters reduce to only four. The somewhat rigid form of the five-parameter distribution function  $f(Q)$  prevents fixing  $\gamma_2$  to  $\gamma_{2e}$ : in order to fit everywhere about equally well, the fitted function does not follow exactly the analytical asymptotic behavior. Alternative solutions to cure this problem are discussed in Appendix B.

Some fits are shown in the lower left panels of Fig. 1, Fig.3 and Fig. 5, and their residuals are shown in the lower panel of Fig.6. The reprojected volume density  $n(r)$  can often fit  $\nu(r)$  satisfactorily for several decades in density with typical residuals  $|\log n(r) - \log \nu(r)| \sim \delta_\nu$  from 0.1 to 0.001 for radius  $0.01 \leq r/B \leq 100$ . Table 5 gives the parameters of the models shown in Fig. 1, Fig. 3 and Fig. 5.

## 5. Re-projected velocity profiles

The projected velocity profiles are the main observable constraints to the dynamical mass distribution of a system. Since the profiles  $L(R, v_z)$  are functions of both projected radius  $R$  and line-of-sight velocity  $v_z$ , one often prefers to use moments of the profiles at selected projected radius as convenient comparisons with observation. For the spherical  $f(E)$  models here, the odd moments such as rotation and skewness are all zero, and most of the information of the profiles are contained in the lowest order even moments, namely,

---

<sup>3</sup> A useful generalization to Osipkov-Merrit models can be obtained by specifying the distribution function  $f = f(Q_a = -E - \eta J^2) = \frac{d}{dQ_a} G_a(Q_a)$ , where  $G_a(Q_a) = G(Q_a) + \eta g(Q_a)$  is a linear function  $\eta$ , and it reduces to  $G(Q)$  for isotropic model. In this case, one can show (with Eq. 4-148 of Binney and Tremaine) that  $n(r)(1 + \eta r^2) = 2\pi\sqrt{2} \int_0^{\Phi(r)} \frac{G(Q_a) + \eta g(Q_a)}{\sqrt{\Phi(r) - Q_a}} dQ_a$ , and  $G(Q_a)$  and  $g(Q_a)$  depend on  $\eta$  only through  $Q_a$ .

the line intensity (presumably proportional to the projected density  $\mu(R)$ ), the dispersion  $\sigma(R)$  and the kurtosis.

There are several ways to represent a profile with the lowest moments. While the Gauss-Hermit expansion (van der Marel and Franx 1993) is mathematically elegant, Zhao and Prada (1996) showed that the direct Gauss-Hermit expansion generically gives rises to profiles with negative wings and multiple peaks. To cure these problems without losing the elegance and many nice properties of the Gauss-Hermit expansion, they proposed the following fitting formula for line profiles, which we will use.

$$L(R, v_z) = \frac{L_0(R)}{\sqrt{2\pi}\sigma} e^{-\frac{v_z^2}{2\sigma(R)^2}} \left\{ 1 + \lambda e^{-\frac{v_z^2}{2\sigma(R)^2}} c_4(R) H_4\left(\lambda \frac{v_z}{\sigma(R)}\right) \right\}, \quad \lambda = \sqrt{\frac{3}{2}}, \quad (27)$$

where  $H_4(y)$  is the four-order Hermit polynomial of  $y$

$$H_4(y) = \frac{2}{\sqrt{6}}(y^4 - 2y^2 + \frac{3}{4}), \quad (28)$$

and  $\sigma(R)$  is the best-fit dispersion at radius  $R$ ,  $c_4(R)$  is a parameter describing the kurtosis of the profile. This fitting formula differs mainly from the usual Gaussian-Hermit expansion by the extra Gaussian damping term  $\sqrt{\frac{3}{2}} e^{-\frac{v_z^2}{2\sigma(R)^2}}$  in front of the Hermit polynomial  $H_4$ , which helps to suppress oscillatory peaks far from systematic velocity and to eliminate the unphysical negative wings; the coefficients  $\sqrt{\frac{3}{2}}$  in the damping term and in the  $H_4$  are to keep the orthogonality of the functions. The formula is robust for mildly double-peaked  $-0.25 \leq c_4 \leq -0.15$  or mildly cuspy  $0.2 \leq c_4 \leq 0.45$  profiles and for profiles close to Gaussian  $-0.1 \leq c_4 \leq 0.1$ . The conventional  $h_4$  parameter is approximately  $c_4$  for nearly Gaussian profiles, but the former cannot fit mildly non-Gaussian profiles.

For the dynamical models here,  $\sigma(R)$  and  $c_4(R)$  are determined by fitting  $L(R, v_z)$  to the projected velocity distribution  $P(R, v_z)$  at each projected radius  $R$ . We minimize the following r.m.s. residual at each radius  $R$ ,

$$\left( \frac{1}{N_v} \sum_{j=0}^{N_v} [L(R, v_j) - P(R, v_j)]^2 \right)^{\frac{1}{2}}, \quad (29)$$

where the velocity grid  $v_j$  and the number of points  $N_v$  is given in Table 1; the velocities  $v_j$  scales with the escape velocity at positions  $R_i$ .

The projected velocity distribution  $P(R, v_z)$  at projected radius  $R$  of the  $f(Q)$  models is simply

$$P(R, v_z) \equiv \int_{-\infty}^{\infty} dz \int \int dv_x dv_y f(Q) \quad (30)$$

$$= 4\pi \int_0^\infty dz G(Q = \Phi(\sqrt{R^2 + z^2}) + \frac{1}{2}v_z^2), \quad (31)$$

where  $G(Q)$  is defined in Eq. 13. So the profile  $P(R, v_z)$  has been reduced from a 3D to a 1D line-of-sight integration. See Appendix C for derivation of this equation and its generalized form for anisotropic systems.

Fig. 2 and 4 show some typical line-of-sight velocity distribution fits at three different radii  $R = 0.1, 1, 10$ . One can see that the fitting formula can recover the profiles  $P(R, v_z)$  to good accuracy. The residual is typically between 0.01 and 0.05 of the peak intensity.

The right panels of Fig.1, Fig.3, and Fig. 5 also show the radial run of the dispersion and kurtosis for a few models. As noted in Tremaine et al. (1994), depending on the strength of the central cusp, the dispersion can have a peak near the break radius (if  $1 \leq \gamma < 2$ ) or a steady falling radial profile (if  $\gamma \geq 2$  or  $\gamma < 1$ ).

## 6. An application to observed galaxies

As an illustration of the models, we apply them to a sample of observed galactic nuclei given in Byun et al (1996). The intrinsic volume density and phase space density parameters of these systems are derived and listed in Table 4.

Interestingly most of observed nuclei have a divergent total mass if the light profile is extrapolated to infinity because their  $\beta = \beta_1 + 1 \leq 3$ . The typical values for  $\alpha_1 \sim 0.5$ . These properties would not be adequately accounted for by a known narrow class of analytical models by Dehnen (1993) and Tremaine et al. (1994), which are characterized with  $\beta = 4$  and  $\alpha = 1$ .

The residuals of our proposed analytical models for the volume density and phase space density of galactic nuclei are about as small as (if not smaller than) the residual for the double-power-law used in Byun et al. fitting the photometric data. We conclude that the universal surface brightness profile also corresponds to a universal volume density and phase space density. And the analytical models here are secure for interpreting observation.

Given this, we can make predictions on observable kinematics. The fitted values of  $\sigma(R)$  and  $c_4(R)$  on a radial grid are given in Table 5. To obtain values at other radius, one can simply interpolate between the tabulated values as both quantities are smooth functions of the radius.

As it is clear from Table 5, the model predicts a very small kurtosis near or outside the break radius of these observed nuclei. We note that this is general as shown in the right

bottom panels of Fig. 1, Fig. 3 and Fig. 5 for hypothetical systems. We find that for the whole class of double-power-law isotropic models with  $0 < \gamma_1 < 2$  and  $\beta_1 \geq [2, \gamma_1]_{max}$  and  $0.5 \leq \alpha_1 \leq 2$ , the profiles are always very close to Gaussian with  $-0.05 < c_4(R) < 0.2$ . The amplitude of  $c_4(R)$  generally increases towards the center, but is small at all radii. Outside the core,  $R \geq 1$ , the kurtosis is negligibly small with  $|c_4(R)| \leq 0.03$ . These results argue that velocity profiles are always very close to Gaussian for the whole class of isotropic double-power-law models. They support the interpretation that strongly non-Gaussian profiles near or inside the break radius are indications of either anisotropy or central black hole.

## 7. Summary

In summary, a large number of galactic nuclei obey a parametrized double-power-law surface brightness radial profile (Byun et al. 1996). We find that their intrinsic volume density fits a similar universal double-power-law with a comparable residual. We further explore spherical isotropic models consistent with these profiles, and find a simple fitting formula for the distribution function  $f(E)$  as well. These parametrizations are tailored so that their functional forms reduce to power-laws at large or small radius.

These analytical models also simplify the procedures to interpret photometric and kinematic data of galactic nuclei. We demonstrate the models with a simple application to a group of observed galactic nuclei, and predict the radial runs of their velocity dispersion and kurtosis. Tables for computed models as well as FORTRAN programs to run additional models are available at site <http://ftp.ibm-1.mpa-garching.mpg.de/pub/hsz>.

Galactic nuclei are generally flattened with a possible central black hole and velocity anisotropy. For these models the distribution function is generally a function of two or three integrals,  $f = f(E, J_z, I_3)$ . Still the simple spherical model here can provide some simple insights which help to build these more complex models. We expect that an  $f(E, J_z, I_3)$  with its energy dependence similar to the fitting formula for isotropic models here will give a plausible fit to anisotropic flattened systems if with a double-power-law radial profile.

I thank Dave Syer for a critical reading of the manuscript and many helpful comments.

## REFERENCES

Binney, J.J., & Tremaine, S., 1987, ‘Galactic Dynamics’ (Princeton University Press, New Jersey).

Byun et al. 1996, SISSA/astro-ph/9602117

Dehnen, W. 1993, MNRAS, 265, 250.

Lauer, T. R., Ajhar, E. A., Byun, Y. I., Dressler, A., Faber, S. M., Grillmair, C., Kormendy, J., Richstone, D., & Tremaine, S. 1995, AJ, 110, 2622

Press, W. et al. 1992, Numerical Recipes in FORTRAN, 2nd. edition, (Cambridge University Press: New York City)

Tremaine, S. et al. 1994, A.J., 107, 2, 634

van der Marel, R. P. & Franx, M., 1993, ApJ, 407, 525

Zhao, H.S. 1996, MNRAS, 278, 488

Zhao, H.S. and Prada, F. 1996, MNRAS, accepted

Zhao, H.S. and Syer, D.. 1996, work in progress

## 8. Appendix

### A. Asymptotic expressions of the double-power-law models

Here we give the asymptotic expressions for the projected density, the phase space density and the potential for the double-power-law *volume* density model.

For the volume density  $\nu(r)$

$$\nu(r) \rightarrow \nu_0 \left(\frac{r}{b}\right)^{-\beta} \text{ if } r \rightarrow +\infty, \quad (\text{A1})$$

$$\rightarrow \nu_0 \left(\frac{r}{b}\right)^{-\gamma} \text{ if } r \rightarrow 0, \quad (\text{A2})$$

For the projected density  $I(R)$

$$I(R) = 2 \int_0^{+\infty} \nu(\sqrt{R^2 + z^2}) dz \quad (\text{A3})$$

$$\rightarrow c_{\beta-1} \left(\frac{R}{b}\right)^{1-\beta} \text{ if } R \rightarrow +\infty \quad (\text{A4})$$

$$\rightarrow I_0 H(1 - \gamma) + c_{\gamma-1} \left(\frac{R}{b}\right)^{1-\gamma} \text{ if } R \rightarrow 0, \quad (\text{A5})$$

where  $H(x)$  is a step function, which is unity for  $x > 0$  and zero otherwise, and

$$c_n = \frac{2\nu_0 b \sqrt{\pi} \Gamma(1 + \frac{n}{2})}{n \Gamma(\frac{1+n}{2})}, \quad n > 0, \quad (\text{A6})$$

and

$$I_0 = 2\nu_0 b \alpha B(\alpha(\beta - 1), \alpha(1 - \gamma)). \quad (\text{A7})$$

For the potential  $\Phi(r)$

$$\frac{\Phi(r)}{4\pi\nu_0 b^2} \rightarrow \alpha \frac{b}{r} B(\alpha(3 - \gamma), \alpha(\beta - 3)) H(\beta - 3) + \frac{1}{(3 - \beta)(\beta - 2)} \left(\frac{b}{r}\right)^{\beta-2} \text{ if } r \rightarrow +\infty \quad (\text{A8})$$

$$\rightarrow \alpha B(\alpha(\beta - 2), \alpha(2 - \gamma)) H(2 - \gamma) + \frac{1}{(3 - \gamma)(\gamma - 2)} \left(\frac{b}{r}\right)^{\gamma-2} \text{ if } r \rightarrow 0 \quad (\text{A9})$$

where  $\beta > [2, \gamma]_{min}$ ,  $0 \leq \gamma < 3$ . The zero point of the potential is at infinitely large radius. The depth of the potential well  $\Phi_0 = \Phi(0) > 0$  is infinite for models with a strong cusp with  $\gamma \geq 2$  (or if there is a central black hole), and is finite for  $\gamma < 2$ .

For the phase space density  $f(Q) = \frac{d}{dQ} G(Q)$ , we have

$$G(Q) = \frac{1}{2\pi^2 \sqrt{2}} \int_{Q \geq \Phi(r)} \frac{d\nu(r)}{dr} \frac{1}{\sqrt{Q - \Phi(r)}} dr \quad (\text{A10})$$

$$\propto q^{\beta_{2e}} \text{ if } Q \rightarrow 0 \quad (\text{A11})$$

$$\propto q^{\gamma_{2e}} \text{ if } Q \rightarrow \Phi(0), \quad (\text{A12})$$

where  $q$  is given in Eq. 14, and

$$\beta_{2e} = \left[ \frac{\beta}{\beta - 2} - \frac{1}{2}, \beta - \frac{1}{2} \right]_{max}, \quad (\text{A13})$$

and

$$\gamma_{2e} = \frac{\gamma + 2}{2|\gamma - 2|} \text{ if } \gamma > 0 \quad (\text{A14})$$

$$= \left[ \frac{1}{2} \left( 1 - \frac{1}{\alpha} \right), 0 \right]_{max} \text{ if } \gamma = 0. \quad (\text{A15})$$

## B. Other Approximate Models

A disadvantage of the fit formulae purposed in the main text for the volume density and the phase space density is that they do not follow rigorously with the analytical asymptotic expressions at small radius. Rather the parameters  $\gamma$  and  $\gamma_2$  are free fitting parameters adjusted to fit all radii equally well. This might be OK for fitting observations with finite resolution at the center, but is not satisfactory for theoretical modelling.

On the other hand, it is possible to devise other expressions which have the expected analytical asymptotic behavior while still keeping the residual small near the transition region.

The projected density  $I(R)$  of the double-power-law density  $\nu(r)$  (cf. Eq. 2, and 5) satisfies the following approximation,

$$I(R) \approx I_{in}(R) + I_{out}(R), \quad (\text{B1})$$

where

$$I_{in}(R) = c_{\gamma-1} \left( \frac{R}{b} \right)^{1-\gamma} \left( 1 + \left( \frac{R}{b} \right)^{\frac{1}{\alpha}} \right)^{-1-\alpha(\beta-\gamma)}, \quad \text{if } \gamma > 1, \quad (\text{B2})$$

and

$$I_{out}(R) = c_{\beta-1} \left( \frac{R}{b} \right)^{1-\gamma+\frac{1}{\alpha}} \left( 1 + \left( \frac{R}{b} \right)^{\frac{1}{\alpha}} \right)^{-1-\alpha(\beta-\gamma)}, \quad (\text{B3})$$

where  $c_n$  is given in Eq. A6.

The approximation is devised so that  $I_{in}(R) + I_{out}(R)$  is rigorously  $I(R)$  at asymptotically big or small radius.

$$I(R) \rightarrow I_{in}(R) \rightarrow c_{\gamma-1} \left( \frac{R}{b} \right)^{1-\gamma} \gg I_{out}(R) \text{ if } R \rightarrow 0, \quad (\text{B4})$$

and

$$I(R) \rightarrow I_{out}(R) \rightarrow c_{\beta-1} \left(\frac{R}{b}\right)^{1-\beta} \gg I_{in}(R) \text{ if } R \rightarrow +\infty . \quad (\text{B5})$$

The approximation is also found to be typically accurate within a 10% in the transition region. This is qualitatively understandable if ones notes the equality

$$\nu_{\alpha,\beta,\gamma}(r) = \nu_{\alpha,\beta+\frac{1}{\alpha},\gamma}(r) + \nu_{\alpha,\beta,\gamma-\frac{1}{\alpha}}(r), \quad (\text{B6})$$

where the subscripts specify the double-power-law slopes, and that the projected density of  $\nu_{\alpha,\beta-\frac{1}{\alpha},\gamma}(r)$  and  $\nu_{\alpha,\beta,\gamma-\frac{1}{\alpha}}(r)$  is roughly  $I_{in}(R)$  and  $I_{out}(R)$  respectively.

The above suggests that it is worthwhile to fit the real photometric data with  $I_{in}(R) + I_{out}(R)$  instead of  $\mu(R)$ , because one obtains simple accurate expressions for the projected density and the volume density simultaneously. But note that if  $\gamma \leq 1$ , namely, if the projected profile has a finite core, the expression for  $I_{in}(R)$  is undefined (because  $c_{\gamma-1}$  is undefined, see Eq. A6).

With similar techniques, one can also work out simple approximation to the phase space density corresponding to the double-power-law. The idea is to write

$$f(Q) = f_{in}(Q) + f_{out}(Q), \quad (\text{B7})$$

so that  $f_{in}(Q)$  is approximately consistent with  $\nu_{\alpha,\beta-\frac{1}{\alpha},\gamma}(r)$  and  $f_{out}(Q)$  with  $\nu_{\alpha,\beta,\gamma-\frac{1}{\alpha}}(r)$ . The results (not given here) are somewhat tedious depending on the range of  $\gamma$  and  $\beta$ .

### C. Line profile expressed as a 1D integral

Here we show that the line profile can be reduced to a 1D integral for the models. With no loss of simplicity we will derive the equations in the slightly general context of a Ospikov-Merritt type anisotropic model, where the distribution function

$$f(E, J) = f(Q_a), \quad Q_a \equiv -E - \frac{1}{2}\eta J^2 \quad (\text{C1})$$

where  $\eta \equiv \frac{1}{r_a^2}$  has the dimension of inverse squared distance, and  $r_a$  is an anisotropy radius. If  $\eta > 0$ , then beyond  $r_a$  most orbits are radial. The model reduces to isotropic with  $f = f(E)$  in the special case that  $\eta = 0$ .

Generally

$$Q_a = \Phi(r) - \frac{1}{2}(v_x^2 + v_y^2 + v_z^2 + \eta J^2), \quad (\text{C2})$$

and

$$J^2 = (xv_y - yv_x)^2 + (xv_z - zv_x)^2 + (zv_y - yv_z)^2, \quad (\text{C3})$$

$$= v_x^2(y^2 + z^2) + v_y^2(x^2 + z^2) + v_z^2(x^2 + y^2) - 2(xyv_xv_y + yzv_yv_z + zxv_zv_x). \quad (\text{C4})$$

Without loss of generality, we can set

$$x = R, \quad y = 0 \quad (\text{C5})$$

It then follows that

$$Q_a = \Phi(r) - \frac{1}{2}(a_R v_z^2 + a_z v_x^2 - 2a_{Rz} v_z v_x + a_r v_y^2) \quad (\text{C6})$$

where

$$a_R = (1 + \eta R^2), \quad a_z = (1 + \eta z^2), \quad a_r = (1 + \eta z^2 + \eta R^2), \quad a_{Rz} = \eta R z. \quad (\text{C7})$$

With a change of variables

$$v_y = v'_y, \quad v_x = v'_x + u, \quad u = \frac{a_{Rz} v_z}{a_z}, \quad (\text{C8})$$

we have

$$dv_x dv_y = dv'_x dv'_y, \quad (\text{C9})$$

and

$$Q_a = \Phi(r) - \frac{1}{2}(v_z^2 a_{rz} + v_x'^2 a_z + v_y'^2 a_r), \quad (\text{C10})$$

where

$$a_{rz} = (a_R - \frac{a_{Rz}^2}{a_z}) = \frac{1 + \eta(R^2 + z^2)}{1 + \eta z^2}. \quad (\text{C11})$$

With a further transformation of coordinates, one finds that

$$\int \int dv_x dv_y f(Q_a) = \int_0^{Q_a} \int_0^{2\pi} d\theta dQ_a f(Q_a) \frac{1}{\sqrt{a_r a_z}}. \quad (\text{C12})$$

If one can devise a function  $G_a(Q_a)$  as an elementary function of  $Q_a$  and specify the phase space density  $f(Q_a)$  by

$$f(Q_a) = \frac{d}{dQ_a} G_a(Q_a), \quad (\text{C13})$$

then the 3D integral for the line profile is reduced to a 1D integral,

$$P(R, v_z) = \int_{-\infty}^{\infty} dz \int \int dv_x dv_y f(Q_a) \quad (\text{C14})$$

$$= 4\pi \int_0^{\infty} dz \frac{G_a(Q_a)}{(1 + \eta(R^2 + z^2))^{1/2} (1 + \eta z^2)^{1/2}}, \quad (\text{C15})$$

where

$$Q_a = \Phi(\sqrt{R^2 + z^2}) - \frac{v_z^2}{2} \frac{1 + \eta(R^2 + z^2)}{1 + \eta z^2}. \quad (\text{C16})$$

When  $\eta = 0$  and  $G_a(Q_a) = G(Q)$ , the above reduces to Equation 30 of isotropic models.

Table 1. Fitting the surface density and volume density at points  $\frac{R_i}{B} = \frac{r_i}{B}$  for  $i = 1, \dots, N_R = N_r = 13$ .

i=1	2	3	4	5	6	7	8	9	10	11	12	13
0.01	0.02	0.05	0.1	0.2	0.5	1	2	5	10	20	50	100

Note. —  $B$  is the break radius of the surface brightness profile.

Table 2. fit the line profiles at the following velocities  $\frac{v_j}{V_{esc}(R)}$  for  $j = 1, \dots, N_v = 10$ .

j=1	2	3	4	5	6	7	8	9	10
0	0.1	0.2	0.3	0.4	0.5	0.6	0.7	0.8	0.9

Note. —  $V_{esc}(R)$  is the escape velocity at radius  $R$ . The fit is done for radii  $R = R_i$  with  $i = 4, \dots, N_R = 13$  as in Table 1.

Table 3. The parameters for models shown in Fig. 1, Fig. 3 and Fig. 5: the surface brightness profile  $(\alpha_1, \beta_1, \gamma_1)$ , the volume density model  $(\alpha, \beta, \gamma, b, \nu_0)$  and its rms residual, the phase space density model  $(\alpha_2, \beta_2, \gamma_2, Q_b, f_0)$  and its rms residual.

$\alpha_1\text{-}\beta_1\text{-}\gamma_1$	$\alpha$	$\beta$	$\gamma$	$b$	$\nu_0$	rms	$\alpha_2$	$\beta_2$	$\gamma_2$	$Q_b$	$\ln f_0$	rms
0.5_1.8_0.0	0.50	2.80	0.00	1.00	0.47	1.E-03	0.64	3.50	0.16	27.80	-7.40	7.E-02
0.5_1.8_0.5	0.50	2.80	1.36	1.36	0.20	3.E-02	0.25	3.50	2.34	18.90	-7.99	2.E-01
0.5_1.8_1.0	0.50	2.80	1.97	1.40	0.19	1.E-02	0.67	3.50	9.99	14.47	-8.66	2.E-01
0.5_1.8_1.5	0.50	2.80	2.49	1.37	0.20	3.E-03	1.87	3.50	5.10	30.13	-8.30	6.E-03
0.5_1.2_0.5	0.63	2.20	1.36	1.26	0.22	3.E-02	1.12	11.00	2.27	13.79	-12.04	1.E-01
0.5_1.8_0.5	0.50	2.80	1.36	1.36	0.20	3.E-02	0.25	3.50	2.34	18.90	-7.99	2.E-01
0.5_2.4_0.5	0.50	3.40	1.33	1.29	0.24	3.E-02	0.25	3.40	2.17	9.49	-7.31	2.E-01
0.5_3.0_0.5	0.50	4.00	1.31	1.23	0.28	4.E-02	0.37	4.00	2.06	3.00	-7.73	7.E-02
0.5_1.4_0.0	0.51	2.40	0.00	1.00	0.40	4.E-03	1.29	6.00	0.00	23.56	-6.54	2.E-02
1.0_1.4_0.0	1.05	2.40	0.26	0.85	0.60	3.E-03	1.27	6.00	0.55	18.72	-7.67	6.E-03
1.5_1.4_0.0	1.57	2.40	0.44	0.79	0.73	2.E-03	1.31	6.00	0.83	17.18	-7.98	2.E-02
2.0_1.4_0.0	2.00	2.40	0.64	0.94	0.47	5.E-03	1.29	6.00	1.11	14.93	-8.40	2.E-02

Note. — The break radius  $B$  and the normalization  $\mu_0$  are set to unity.  $(\alpha_1, \beta_1, \gamma_1)$  and  $(\alpha, \beta, \gamma)$  describe the width of the transition region, the slope of the outer power-law and inner power-law for the surface brightness profile and for the volume density profile.  $b$  and  $\nu_0$  are the scales for the radius and the volume density.

Table 4. For each galaxy the table gives surface bright profile parameters  $(\alpha_1, \beta_1, \gamma_1)$ ‡ found by Byun et al. (1996) by fitting observation, the five volume density model parameters  $(\alpha, \beta, \gamma, b, \nu_0)$ , the five phase space density model parameters  $(\alpha_2, \beta_2, \gamma_2, Q_b, f_0)$  found here. The last column shows the rms residuals (multiplied by 100) of Byun et al. fit, of our volume density model, of our phase space density model respectively.

Galaxy	$\alpha_1$ - $\beta_1$ - $\gamma_1$	$\alpha$	$\beta$	$\gamma$	$b$	$\nu_0$	$\alpha_2$	$\beta_2$	$\gamma_2$	$Q_b$	$\ln f_0$	RMS
N 596	1.3_2.0_0.6	1.29	2.97	1.47	1.32	0.22	0.79	2.57	3.25	2E-3	-25.6	3:0:2
N 720	0.4_1.7_0.1	0.37	2.66	0.44	1.22	0.26	0.75	3.53	0.64	17.6	-8.17	1:0:0
N1172	0.7_1.6_1.0	0.64	2.64	1.98	1.40	0.18	0.47	3.63	9.99	13.0	-8.54	3:0:4
N1399	0.7_1.7_0.1	0.63	2.68	0.52	1.15	0.31	0.70	3.43	0.77	18.3	-8.07	1:0:0
N1400	0.7_1.3_0.0	0.74	2.32	0.13	0.92	0.47	1.31	6.77	0.32	20.0	-7.45	3:0:0
N1600	0.8_2.2_0.0	0.81	3.18	0.20	0.94	0.64	0.40	2.68	0.54	16.8	-6.90	2:0:4
N1700	1.1_1.3_0.0	1.14	2.30	0.35	0.88	0.52	1.34	7.10	0.64	17.7	-8.27	2:0:0
N2832	0.5_1.4_0.0	0.54	2.40	0.23	1.07	0.34	1.13	5.51	0.40	19.2	-7.80	1:0:0
N3115	0.7_1.4_0.8	0.67	2.43	1.75	1.46	0.16	0.35	5.16	4.78	0.92	-20.4	2:0:4
N3377	0.5_1.3_0.3	0.41	2.33	1.12	1.55	0.14	0.81	6.52	1.63	13.6	-10.7	3:0:0
N3379	0.6_1.4_0.2	0.55	2.43	0.89	1.40	0.18	0.90	5.13	1.20	13.9	-9.35	2:0:0
N3608	1.0_1.3_0.0	0.98	2.33	0.27	0.89	0.51	1.31	6.56	0.53	18.3	-7.94	2:0:0
N4168	1.1_1.5_0.1	1.04	2.50	0.80	1.17	0.28	1.00	4.50	1.14	15.9	-8.35	2:0:0
N4365	0.5_1.3_0.1	0.40	2.27	0.81	1.44	0.16	0.93	7.91	1.06	17.8	-10.2	2:0:1
N4464	0.6_1.7_0.9	0.55	2.68	1.85	1.45	0.17	0.86	3.43	9.99	44.9	-5.75	2:0:1
N4551	0.3_1.2_0.8	0.30	2.23	1.77	1.52	0.14	0.16	9.08	5.77	11.1	-16.4	3:0:2
N4552	0.7_1.3_0.0	0.70	2.30	0.10	0.93	0.45	1.33	7.23	0.27	20.5	-7.34	4:0:0
N4621	5.3_1.7_0.5	5.44	2.71	1.43	1.04	0.44	0.59	3.32	5.52	8E-3	-24.6	3:0:0
N4636	0.6_1.3_0.1	0.55	2.33	0.75	1.34	0.19	0.98	6.58	1.00	16.2	-9.52	1:0:0
N4649	0.5_1.3_0.2	0.41	2.30	0.82	1.44	0.17	0.92	7.17	1.08	16.5	-10.0	3:0:1
N4874	0.4_1.4_0.1	0.33	2.37	0.76	1.42	0.17	0.93	5.96	0.98	14.9	-9.45	1:0:1
N4881	0.6_1.4_0.8	0.53	2.36	1.71	1.50	0.15	0.58	6.09	4.71	1.91	-19.1	3:0:2
N4889	0.4_1.3_0.0	0.33	2.35	0.36	1.23	0.24	1.07	6.25	0.51	17.9	-8.42	1:0:1
N5813	0.5_1.3_0.1	0.41	2.33	0.54	1.29	0.22	1.01	6.64	0.73	17.4	-9.06	2:0:1
N5845	0.8_2.7_0.5	0.74	3.74	1.36	1.24	0.26	0.27	3.24	2.32	3.21	-7.40	8:0:0

Note. — The  $\alpha_1$  here is the inverse of the  $\alpha$  used by Byun et al. (1996). Dimensional quantities are normalized with  $B$  and  $\mu_0$ .  $(\alpha_1, \beta_1, \gamma_1)$  and  $(\alpha, \beta, \gamma)$  describe the width of the transition region, the slope of the outer power-law and inner power-law for the surface brightness profile and for the volume density profile.  $b$  and  $\nu_0$  are the scales for the radius and the volume density.

Table 5. The predicted line-of-sight velocity dispersions  $\sigma(R)$  and kurtosis parameter  $c_4(R)$  at radii  $R/B = 0.1, 0.2, 0.5, 1, 2, 5, 10, 20, 50, 100$ .

Galaxy	$\sigma : 0.1$	0.2	0.5	1	2	5	10	100	$c_4 : 0.1$	0.2	0.5	$ c_4(\geq 1) $
N 596	0.67	0.72	0.74	0.72	0.67	0.57	0.49	0.23	0.02	0.01	0.00	0.02
N 720	0.77	0.84	0.93	0.97	0.95	0.85	0.75	0.42	0.18	0.11	0.04	0.02
N1172	1.41	1.36	1.28	1.20	1.11	0.96	0.82	0.45	-0.01	-0.01	-0.01	0.02
N1399	0.67	0.74	0.83	0.86	0.85	0.78	0.70	0.40	0.17	0.09	0.03	0.02
N1400	0.74	0.78	0.86	0.92	0.97	0.98	0.95	0.75	0.13	0.10	0.05	0.02
N1600	0.61	0.64	0.65	0.63	0.62	0.55	0.46	0.20	0.08	0.03	-0.01	0.02
N1700	0.55	0.62	0.72	0.79	0.85	0.89	0.89	0.75	0.14	0.10	0.05	0.03
N2832	0.79	0.84	0.92	0.97	1.00	0.97	0.91	0.65	0.15	0.10	0.04	0.02
N3115	1.10	1.13	1.14	1.13	1.09	1.01	0.92	0.62	0.01	0.01	0.00	0.02
N3377	0.69	0.81	0.96	1.05	1.09	1.06	0.99	0.72	0.11	0.08	0.05	0.02
N3379	0.66	0.76	0.89	0.97	1.00	0.96	0.88	0.60	0.15	0.10	0.05	0.02
N3608	0.61	0.67	0.77	0.83	0.89	0.91	0.90	0.72	0.14	0.10	0.05	0.03
N4168	0.55	0.63	0.73	0.78	0.81	0.79	0.75	0.52	0.12	0.08	0.03	0.02
N4365	0.68	0.81	0.95	1.05	1.11	1.10	1.05	0.81	0.17	0.12	0.06	0.03
N4464	1.20	1.21	1.19	1.15	1.07	0.91	0.78	0.42	0.00	0.00	-0.00	0.02
N4551	1.11	1.16	1.20	1.23	1.23	1.20	1.15	0.87	0.01	0.01	0.01	0.02
N4552	0.78	0.81	0.88	0.94	0.99	1.01	0.98	0.79	0.12	0.09	0.05	0.02
N4621	0.15	0.15	0.15	0.15	0.15	0.14	0.13	0.10	0.00	0.00	-0.00	0.02
N4636	0.67	0.77	0.91	0.99	1.04	1.02	0.97	0.73	0.16	0.12	0.06	0.02
N4649	0.68	0.80	0.95	1.04	1.09	1.07	1.01	0.77	0.16	0.12	0.06	0.02
N4874	0.71	0.81	0.95	1.04	1.08	1.04	0.97	0.69	0.19	0.13	0.06	0.02
N4881	1.05	1.09	1.14	1.15	1.14	1.07	1.00	0.72	0.01	0.01	0.00	0.02
N4889	0.82	0.88	0.98	1.06	1.09	1.05	0.98	0.72	0.19	0.13	0.06	0.02
N5813	0.75	0.83	0.95	1.04	1.08	1.05	0.99	0.74	0.20	0.14	0.06	0.02
N5845	0.74	0.79	0.81	0.75	0.63	0.46	0.35	0.12	0.03	0.02	-0.00	0.02

Note. — The last column is the maximum of  $|c_4(R)|$  outside the core  $R \geq 1$ . The dispersion  $\sigma$  is normalized with  $(G\mu_0 B)^{\frac{1}{2}}$ , where  $\mu_0$  and  $B$  are defined in Eq.(1) and  $G$  is the gravitational constant.

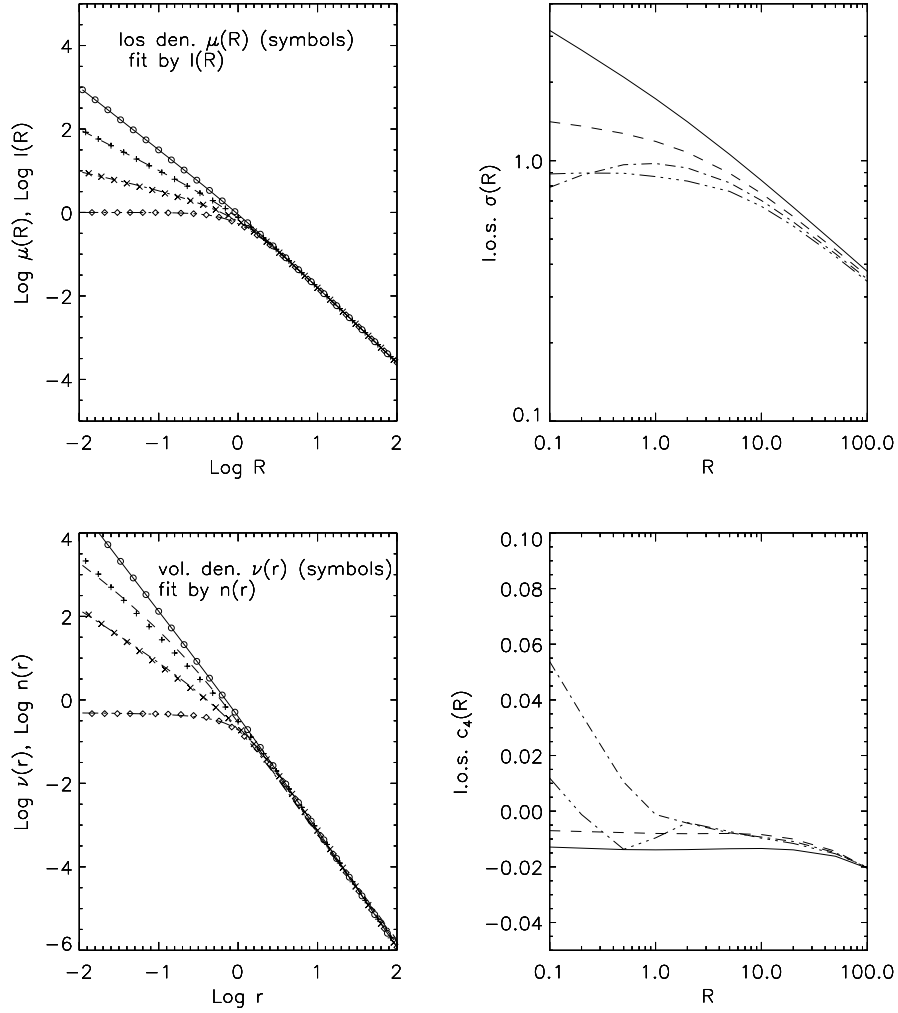


Fig. 1.— shows a) several fits to the surface brightness profiles  $\mu(R)$  by integrating the double-power-law model volume density models, b) several fits to the volume density profiles  $\nu(r)$  by integrating the phase space density models, c) the radial run of the predicted line-of-sight dispersion  $\sigma(R)$  and d) kurtosis  $c_4(R)$  for the isotropic double-power-law dynamical model. The four models have  $(\alpha_1, \beta_1, \gamma_1) = (0.5, 1.8, \gamma_1)$  and  $\gamma_1 = 0, 0.5, 1, 1.5$ , which are shown by the fit of four different type of lines (solid, dashed, dash dot, and dash dot dot dot lines) to four different symbols (circles, pluses, crosses, and diamonds) respectively.

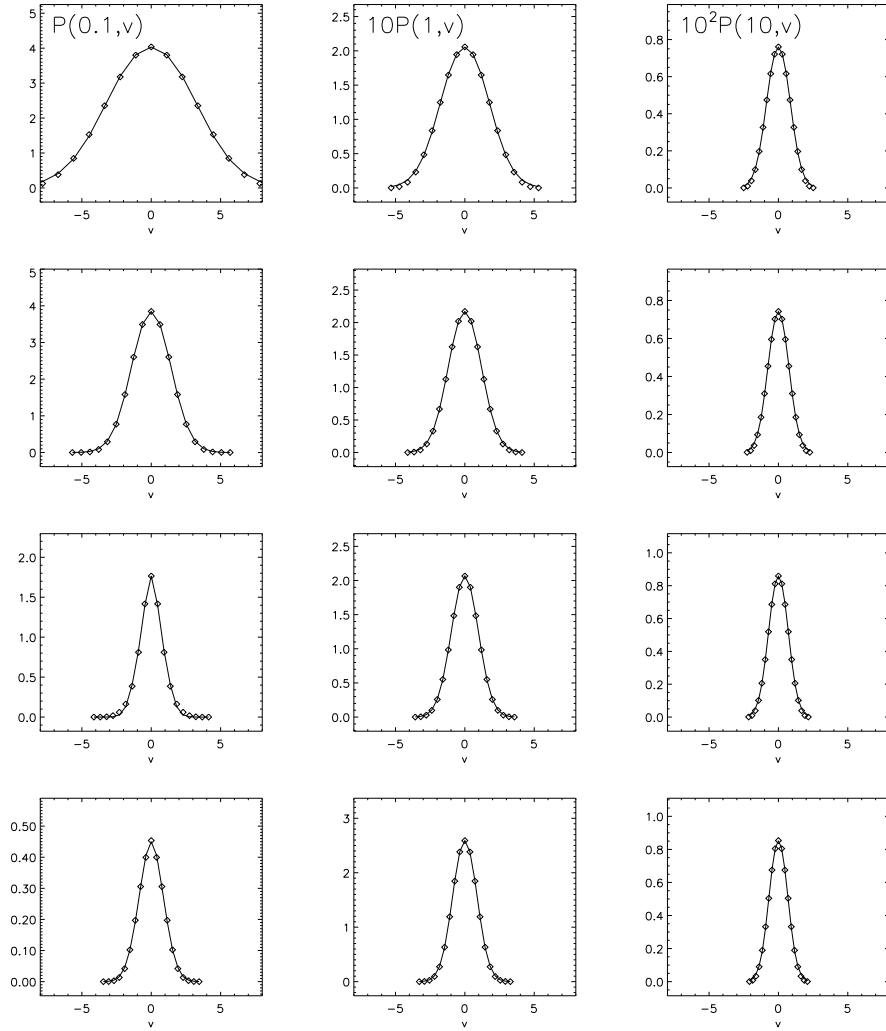


Fig. 2.— from top to down shows the fits to the line profiles of the models shown in Fig.1 with the parameterization by Zhao and Prada (1996). The three columns correspond to profiles at projected radius  $R = 0.1, 1, 10$  from left to right. All models have nearly Gaussian profiles.

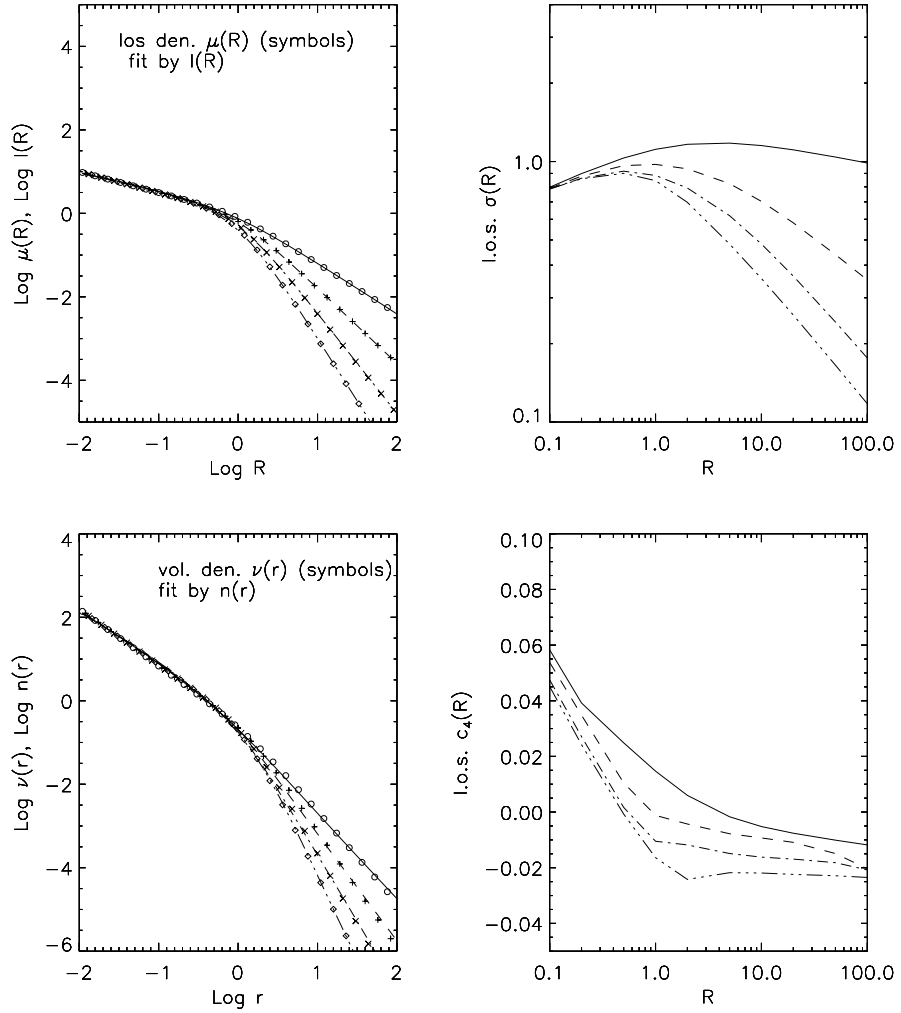


Fig. 3.— similar to Fig.1 except that models have  $(\alpha_1, \beta_1, \gamma_1) = (0.5, \beta_1, 0.5)$  and  $\beta_1 = 1.2, 1.8, 2.4, 3.$

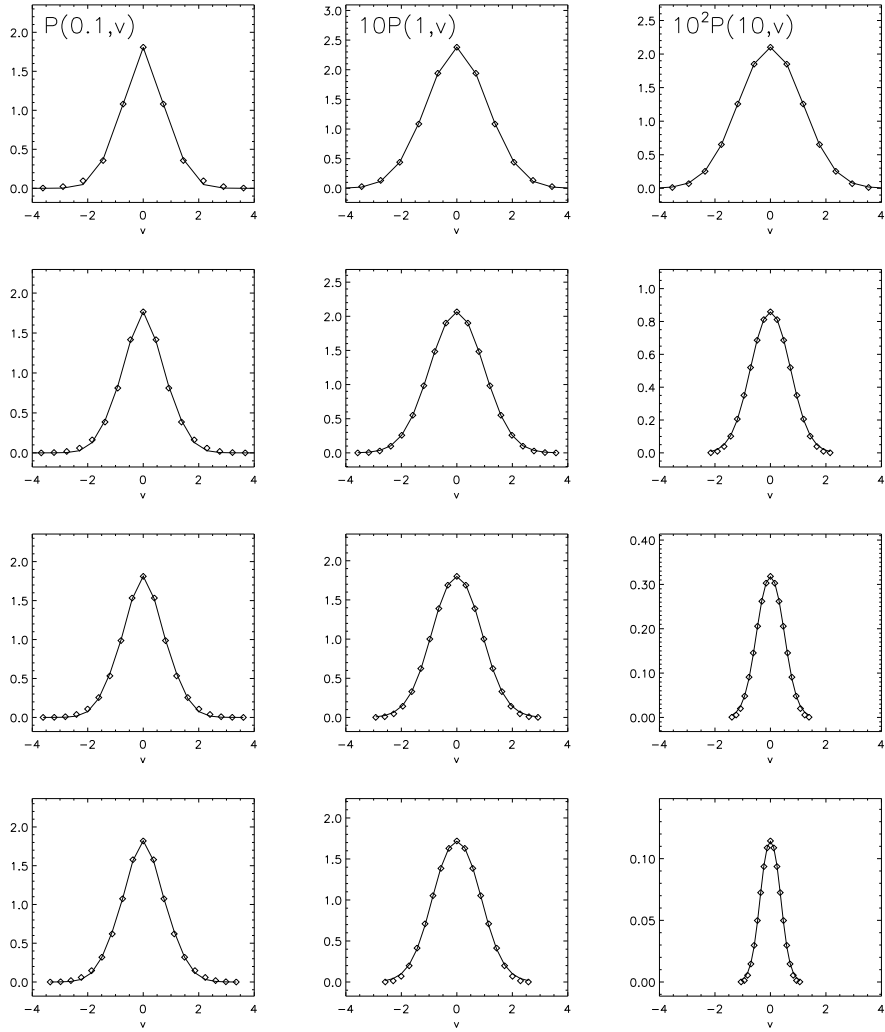


Fig. 4.— similar to Fig.2 except that the models are those in Fig.3.

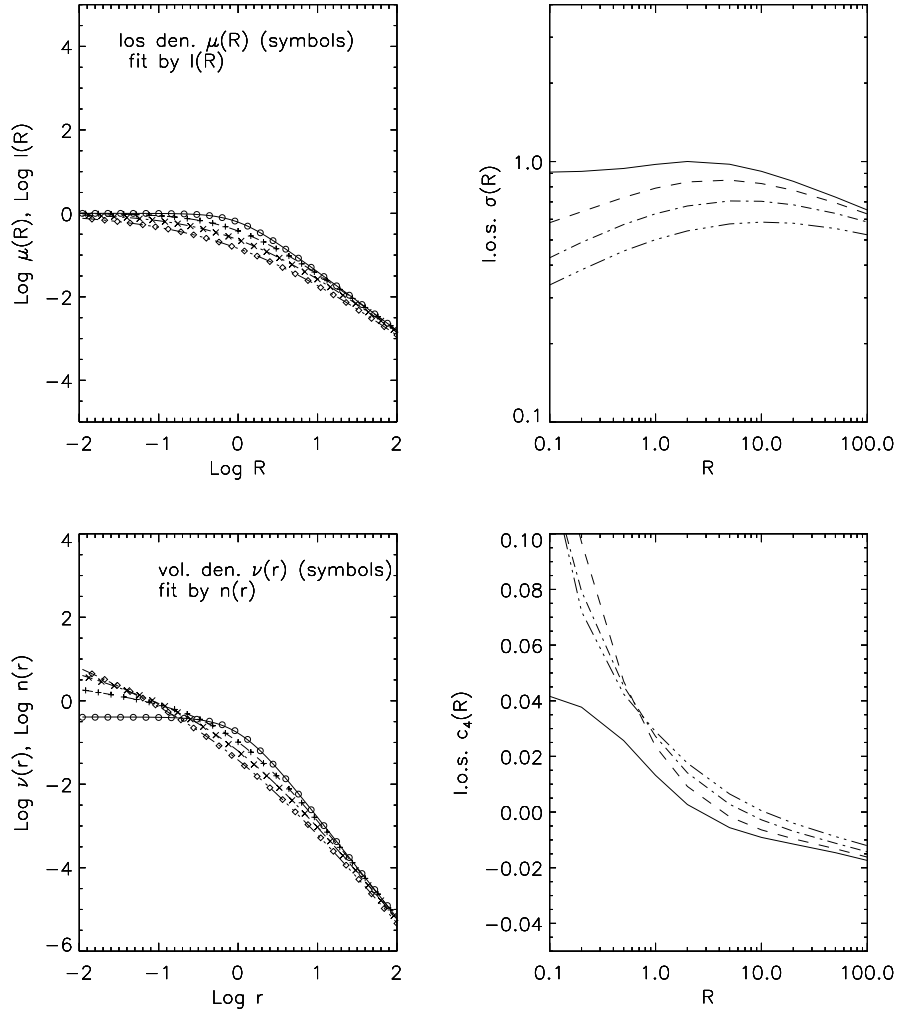


Fig. 5.— similar to Fig.1 except that models have  $(\alpha_1, \beta_1, \gamma_1) = (\alpha_1, 1.4, 0)$  and  $\alpha_1 = 0.5, 1, 1.5, 2..$

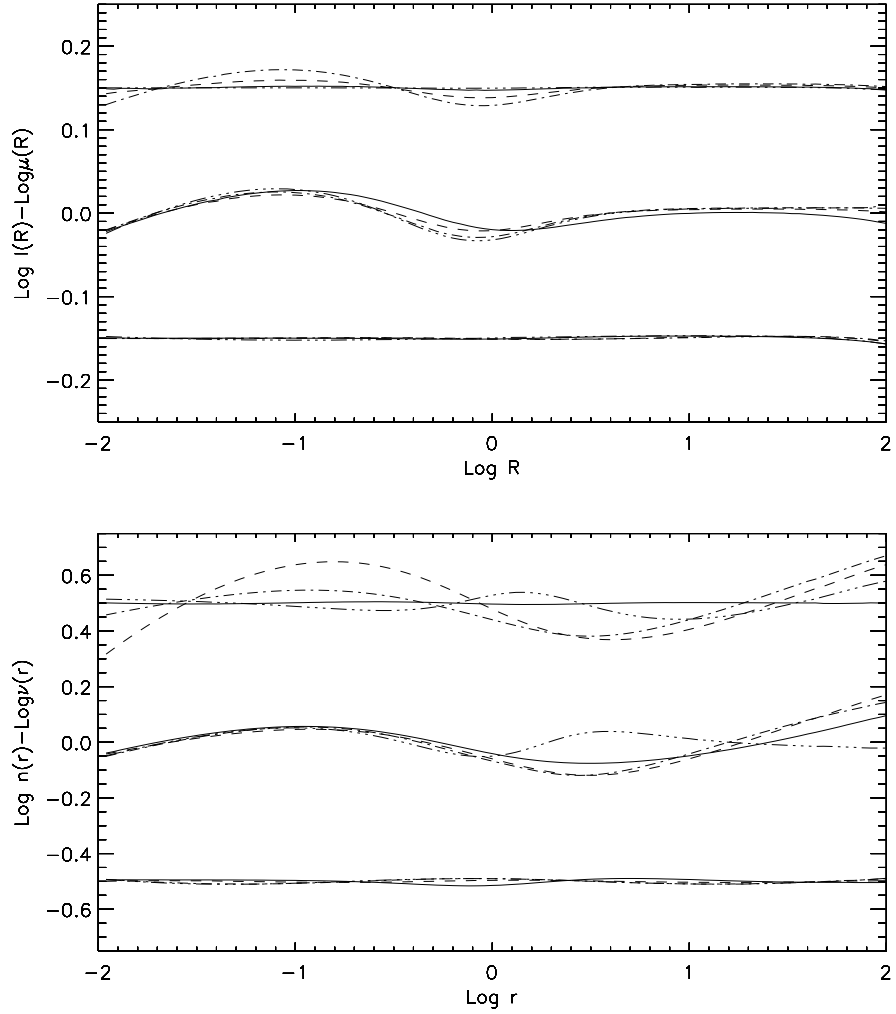


Fig. 6.— from top to down shows the residual as a run of radius of the models in Table 3 for the surface density (upper panel) and the volume density (lower panel). For clarity, the residual of three sets of models has been offset by  $\pm 0.15$  for surface density and  $\pm 0.5$  for volume density.